D_2 desorption kinetics on amorphous solid water: from compact to porous ice films

Jean-Hugues Fillion,*† Lionel Amiaud,‡ Emanuele Congiu, François Dulieu, Anouchah Momeni‡ and Jean-Louis Lemaire

Received 16th December 2008, Accepted 2nd March 2009
First published as an Advance Article on the web 26th March 2009
DOI: 10.1039/b822492g

The desorption kinetics of D_2 from amorphous solid water (ASW) films have been studied by the temperature-programmed desorption (TPD) technique in the 10–30 K temperature range. Compact (and nonporous) films were grown at 120 K over a copper substrate. Ultra-thin porous films were additionally grown at 10 K over the compact base. The TPD spectra from compact and from up to 20 monolayers (ML) porous films were compared. The simulation of the TPD experimental traces provides the corresponding D_2 binding-energy distributions. As compared to the compact case, the binding-energy distribution found for the 10 ML porous film clearly extends to higher energies. To study the transition from compact to porous ice, porous films of intermediate thicknesses (<10 ML), including ultra-thin films (<1 ML), were grown over the compact substrate. The thermal D_2 desorption peak was found to shift to higher temperatures as the porous ice network was progressively formed. This behavior can be explained by the formation of more energetic binding sites related to porous films. TPD spectra were also modelled by using a combination of the two energy distributions, one associated to a bare compact ice and the other associated to a 10 ML porous ice film. This analysis reveals a very fast evolution of the binding-energy distribution towards that of porous ice. Our results show that few ML of additional porous film are sufficient to produce a sample for which the D_2 adsorption can be described by the energy distribution found for the 10 ML porous film. These experiments then provide evidence that the binding energy of D_2 on ASW ice is primarily governed by the topological and morphological disorder of the surface at molecular scale.

Introduction

Water is ubiquitous in space and is by far the most abundant condensed-phase species observed throughout the Universe.[1] In low-temperature astrophysical environments (T < 50 K), amorphous forms of water-rich ices are probably dominant, either as a result of the particular conditions of their formation, or due to processes occurring after formation (*e.g.* pressure deformation, processing by photons or cosmic rays).[2–5] Physical and chemical processes of astrophysical ices (sublimation, desorption of impurities, heterogeneous chemistry) are known to play an important role in the chemical and dynamical evolution of the interstellar medium (ISM).[6] Of particular interest are: adsorption, diffusion, chemical reactions and desorption of atoms and molecules occurring at the surface of icy mantles on dust grains. These elementary processes are governed to a large extent by the ice morphology. For example, it has been recently shown that atomic hydrogen recombination occurring at the surface of nonporous amorphous solid water (ASW) releases vibrationally excited molecules in the gas phase, while this behaviour was not observed from porous ASW samples.[7] ASW is generally considered, up to now, as a good laboratory analogue of astrophysical ices. Understanding the structure of ASW, and more specifically the role of its morphology in the gas–ice interaction, is therefore particularly relevant to the context of astrochemistry.

In the laboratory, ASW can be produced under high-vacuum conditions by slow vapour condensation onto a cold substrate (T < 130 K). The physical properties of such water ice (density, refractive index, thermal conductivity, and related morphology) are strongly dependent on the experimental conditions. By changing the experimental deposition method, it is possible to form either porous or compact ice deposits. Especially, the angular distribution of the water molecules during the deposition step is known to play a dramatic role.[8–12] When gas-phase water is introduced into the entire vacuum chamber through a leak valve (“background deposition” technique, commonly used in laboratories), the morphology of the ice grown at low deposition rates (typically <0.5 ML s^{-1}) is extremely sensitive to the substrate temperature. Porosity and average density can be continuously varied by changing the deposition temperature, low temperatures favouring high porosity and low average density.[12] Background deposition of water at high temperatures in the

LERMA-LAMAp, UMR CNRS 8112, Université Cergy-Pontoise et Observatoire de Paris, 5 Mail Gay-Lussac, F-95000, Cergy-Pontoise, France. E-mail: jean-hugues.fillion@upmc.fr; Tel: +33 (0)1 44279605
† Present address: UPMC Univ Paris 06, LPMAA, CNRS UMR 7092, 4 Place Jussieu, box 76, Paris, France.
‡ Present address: Université Paris-Sud, LCAM, CNRS UMR8625, 91405, Orsay Cedex, France.

range 110–120 K produces compact films ($\rho \sim 0.8$–0.9 g cm^{-3}). These films are stable when lowering the temperature subsequently to the formation step. When the deposition step is performed by background deposition at lower temperatures ($T < 110$ K), porous ASW films having much lower average densities ($0.9 \geq \rho \geq 0.6$ g cm^{-3}) are grown.[12] Such films undergo an irreversible densification upon annealing.[12] Extensive experimental studies demonstrate that this evolution is associated to a gradual destruction of the porous network, which can lead to a partial trapping of gas, initially adsorbed on top of the sample surface.[13–15]

In the context of the gas–surface interaction, an important property differentiating porous from compact films is the equivalent surface area available for adsorption that can reach a few thousands of m^2 g^{-1} in the case of highly porous films.[10,16] Depending on the specific preparation method, compact films may contain closed pores that are not interconnected and not open to the external film surface.[10] The surface area available for the adsorption is therefore restricted to the geometric external area of the film in the case of compact films. The surface of compact films, although possibly highly corrugated, can therefore be considered as nonporous. We also stress that this study is concerned with ASW prepared by background deposition. As far as the morphology is concerned, experiments in which similar ASW films are produced by other well-controlled techniques, such as collimated molecular beams or co-deposition of water–rare-gas mixtures followed by annealing, should be compared with care to the results presented here.

In order to probe porous ASW, temperature-programmed desorption experiments (TPD) have been widely used with various gases,[14,17–20] but few are concerned with molecular hydrogen.[21–25] This molecule is particularly weakly bound to the surface and desorption occurs below 30 K. This temperature limit is not high enough to induce severe transformation of the ice structure, neither in the bulk ice, as observed by X-ray electron diffraction spectroscopy,[26] nor at its surface, as proven by TPD experiments.[23] Unlike other gases, diffusion of molecular hydrogen at surface and/or within the connected network of pores is efficient at low temperatures,[27] which is an important parameter when porous and thick samples are probed. One can conclude that TPD experiments performed with molecular hydrogen are well-suited for probing the surface of compact or porous ASW films at low temperatures.

In the present study, because the main residual gas present in the vacuum chamber consists of H_2, surfaces were probed using molecular deuterium (D_2) instead of H_2, enhancing the S/N ratio of the signal detected by the QMS, especially at very low exposures. We have previously shown that TPD spectra of these isotopes are actually almost identical and provide equivalent information, although we also demonstrated that the desorption kinetics can be strongly affected if significant amount of both species are present together on the surface.[28] The interaction of molecular hydrogen (H_2 or D_2) with ASW is indeed characterized by a large distribution of adsorption energies, reflecting the high heterogeneity of the surface. The D_2 TPD spectra are consequently very broad and very sensitive to D_2 coverage, making experimental investigations at variable D_2 exposures necessary to interpret most experiments.[24]

In a previous study, we have proposed a simple statistical approach to model the distribution of molecular hydrogen on their adsorption sites and its dependence with surface temperature and coverage.[24] This approach provides a master curve for the binding-energy distribution that can be used to simulate the desorption kinetics. The validity of such approach was strengthened by the simulation of complex TPD spectra obtained with various admixtures of molecular hydrogen isotopes.[21,28]

In a preceding paper, Hornekaer *et al*, [23] have shown that TPD experiments using molecular hydrogen (D_2) are sensitive to the morphology of ASW. It was shown that the desorption kinetics was affected by the diffusion within the porous network of thick ASW samples (<2000 ML). In particular, the shift of the thermal desorption peak to higher temperatures with increasing porous-ASW ice thickness could be simulated by rescaling the number of molecules close to the external surface area. More recently, Zubkov *et al*.[29,30] have performed N_2 TPD experiments combined with reflection–absorption infrared spectroscopy and molecular beam technique to investigate the desorption kinetics from ASW films of controlled porosity and various thicknesses. These results quantitatively demonstrate the fundamental role of the molecular diffusion (either uniform or non-uniform) in the desorption kinetics.

In this paper, investigations are focused on ultra-thin porous ASW layers ($\leq$20 ML). TPD experiments using molecular hydrogen (D_2) are compared. Based on our statistical model for the adsorption and desorption of molecular hydrogen, the TPD spectra observed at various D_2 exposures could be simulated, providing the binding-energy distributions associated with either a 10 ML porous or compact (nonporous) ASW film, or a combination of the two. The transition from nonporous- towards porous-ice adsorption properties is studied by progressively growing the porous layer over a previously prepared compact substrate. Supported by the model just mentioned above, the binding-energy distributions characterising each porous ice surface can be systematically calculated, enabling to follow their evolution as the new ice network is progressively developing. We show that the surface morphology of an ultra-thin layer of ASW ice can affect dramatically the desorption kinetics of molecular hydrogen on ASW.

Experiment

The experiments were done with the "FORMOLISM" apparatus (FORmation of MOLecules in the InterStellar Medium) developed for studying heterogeneous chemistry on surfaces relevant to astrophysics. Only parts of the system which are useful for the present study are briefly described below. The experiments were performed in a ultra-high vacuum chamber (base pressure $\sim 10^{-10}$ mbar). ASW films are grown on an oxygen-free high-conductivity (OFHC) copper cylinder block, cooled by a closed-cycle He cryostat (ARS Displex DE-204S). The temperature is controlled by a calibrated Silicon-diode sensor and a thermocouple (AuFe/Chromel K-type) clamped on the sample holder and measured with an accuracy of ± 1 K. The H_2O vapour is

obtained from deionized water previously purified by several freeze–pump–thaw cycles carried out under vacuum. A first H_2O ice film was grown using a microchannel array doser installed 2 cm away from the copper surface maintained at 120 K. This arrangement is used to prepare a relatively thick sample of compact water ice ($\sim$150 ML) in order to avoid any perturbations coming from the copper substrate and to get a first hydrophilic substrate over which another type of ASW film is grown. The compact ASW film is cooled down to 10 K before being characterised by TPD (see below). Then the following technique is used to produce the highly porous film: water vapour is introduced through a leak valve to condense on top of the previous ASW thick substrate held at 10 K. The total pressure never exceeds 10^{-8} mbar during this deposition step. The outer layer of added water is grown at a rate that does not exceed 0.003 ML s^{-1} at low background pressure ($<10^{-9}$ mbar). The calculation of water coverage is made by monitoring in real time the water partial pressure and by assuming perfect sticking at these low temperatures.[31] Each new sample is probed by a series of D_2 TPD experiments performed with several D_2 doses.

A typical TPD experiment is decomposed in three steps. Firstly, the sample undergoes a heating–cooling cycle (10 K–30 K–10 K) without probing gas (dry-run), in order to stabilize the surface morphology before subsequent heating sequences. This is done to ensure that all the TPDs, including the first series, are performed on the same type of substrate, namely a sample annealed to 30 K. Secondly, a room-temperature normal mixture of *ortho*-D_2 and *para*-D_2 is introduced through a leak valve at a rate of $\sim$0.001 ML s^{-1}. Exposures are carefully controlled by monitoring the D_2 partial pressure in the chamber with a quadrupole mass spectrometer (QMS, HIDEN 3F/PIC) together with an ionization pressure gauge. The ASW film is maintained at 10 K during the deposition. Finally, the QMS is translated to a position 3 mm in front of the surface for TPD measurements. D_2 desorption rates are measured during the linear heating ramp (0.17 K s^{-1}). The temperature of the ASW samples never exceeds 30 K during all these experiments.

Results

A Compact and porous ice films

Fig. 1a shows a series of D_2 TPD spectra recorded from a $\sim$150 ML compact ASW film. The film was prepared, as indicated before, by growing the ASW film at 120 K prior to being cooled to 10 K. Thereby, the structure of the ice film is believed to be very compact and the surface is nonporous. The corresponding TPD spectra are compared with those obtained from a 10 ML porous ASW film prepared at 10 K by slow vapour condensation (Fig. 1b). In both cases, films are exposed to molecular hydrogen (D_2) by background pressure at room-temperature (see experimental section above). The number of molecules hitting the surface is calculated by monitoring the D_2 partial pressure in the vacuum chamber during the deposition phase. Doses and desorption fluxes are given in terms of monolayers and monolayers per second, respectively, where 1 ML = 10^{15} molecules cm^{-2}. This unit

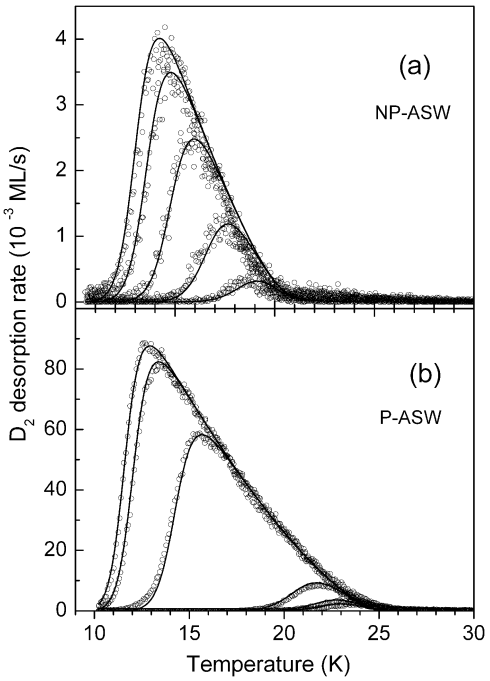

Fig. 1 Temperature-programmed desorption of D_2 from (a) compact nonporous ASW (NP-ASW) (b) 10-ML porous ASW (P-ASW). Circles are experimental data and solid lines are simulations based on a statistical model (see text for details). The compact film is prepared by growing 150 ML of ASW at 120 K prior to being cooled to 10 K. The highly porous film is grown onto the compact base at 10 K. D_2 exposures are expressed in ML where 1 ML = 10^{15} molecules cm^{-2}. The exposures are displayed by increasing order: (a) 0.02, 0.1, 0.26, 0.41, 0.5 ML D_2; (b) 0.04, 0.07, 0.2, 3.5, 4 ML D_2. Exposures are obtained by monitoring the D_2 partial pressure with time and assuming perfect sticking efficiency.

approximates the water surface density of crystalline ice. Doses represent the density that would be present at the surface if every molecule that hits the surface would stick. It is not expected that 1 ML of D_2 exposure would actually correspond to one monolayer completion, both because the nonporous surface can be highly corrugated with respect to the crystalline case and because the sticking is not perfectly efficient. As seen previously,[23] the effective available surface for adsorption on ASW can indeed exceed 1 ML. In the absence of D_2 multilayer signatures in the TPD spectra (that would require temperatures lower than 10 K), absolute coverage calibration was unfortunately not possible in the present study. In particular because the sticking efficiency is variable with coverage and ice thickness,[7] exposures should rather be taken as maximum values for the D_2 coverage actually adsorbed on the surface. Nevertheless, we believe that absolute D_2 coverage remains low during all the present experiments. Indeed, the area under the TPD curves, increases quasi-linearly with exposure and reaches a maximum when the accommodation of molecules at the surface saturates. In the case of the compact nonporous surface for example, this maximum was found to occur close to 0.5 ML exposure. Considering a maximum sticking efficiency of $\sim$0.5, one can estimate that the coverage of the total surface area cannot have exceeded 25% in our experiment.

The desorption rates measured from the 10 ML porous surface are found to be about 20 times those measured from the nonporous surface (Fig. 1). This illustrates the important increase of the effective surface area available for adsorption when comparing nonporous and porous surfaces. Besides this fundamental difference, the general behaviour of the TPD spectra after D_2 doses is very similar in both cases: as the D_2 coverage increases, the TPD curves keep growing and broadening to the lowest temperatures, keeping at higher temperature a common trailing edge at any D_2 exposures. This peculiar evolution of the TPD spectra with D_2 coverage is correlated with the high mobility of hydrogen molecules on the surface and to a sequential occupancy of a wide distribution of adsorption sites. Such a signature is very characteristic of the strong heterogeneity of ASW, as also seen at higher temperatures.[10] In addition to the strong difference in the desorption rates, the shapes of the TPD spectra arising from nonporous and porous surfaces are not identical. Clearly, no significant desorption is measured above 21 K from the compact surface, whereas desorption from the porous surface persists up to 25 K and slightly above.

In order to get a more quantitative view of the distribution of adsorption energies underlying these broad TPD curves, we have employed a fitting-based procedure to model the series of TPD spectra. The method used to obtain the binding-energy distribution of molecular hydrogen interacting with ASW has been discussed in a previous publication[24] and is only briefly reviewed here. The binding-energy distribution is described by a polynomial function $g(E) = a(E_0 - E)^b$ for $E < E_0$, where a, E_0 and b are parameters to be determined from the TPD analysis. At a given temperature and a given coverage, this distribution is assumed to be populated following a Fermi–Dirac statistical law. This is appropriate considering that one adsorption site can be filled by one molecule solely and by assuming high mobility on the surface. In a second step of the calculations, we simulate the heating of the sample by calculating first order thermal desorption rates expressed in terms of a classical Arrhenius law: $R(\theta) = -\mathrm{d}\theta/\mathrm{d}t = A(\theta)\theta \exp[-E(\theta)/kT]$, where R is the desorption rate, θ the adsorbate coverage, E the binding energy, t the time, $A = 10^{13}$ s^{-1} the pre-exponential factor of desorption, T the sample temperature and k the Boltzmann constant. The population distribution is continuously (re)calculated at each temperature increment. The parameters defining the curve $g(E)$ are adjusted by using a least-squares fitting approach (Levenberg–Marquardt or similar non-linear fitting procedure) over the whole set of desorption curves. The agreement between simulated and experimental TPD curves is illustrated in Fig. 1. The energy distribution function $g_1(E)$ characterizing the compact film is shown in solid line in Fig. 2. The function $g_2(E)$ characterising that of the porous surface is displayed in dotted line for comparison. No information for the presence of adsorption sites below 30 meV can be obtained in the present investigations. Experiments conducted at lower temperature and higher coverage are in fact required for that purpose. For both functions, half of the adsorption sites are found to lie above 40 meV. Clearly, the distribution obtained from compact ice is confined below 60 meV whereas that of porous ice presents a tail extending slightly above 70 meV.

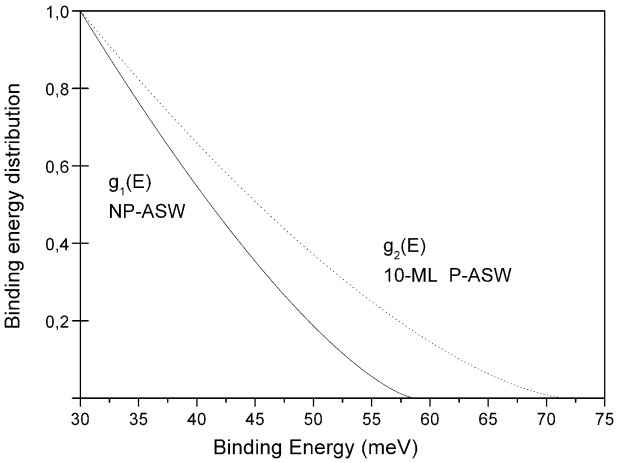

Fig. 2 Binding-energy distribution for compact ice ($g_1(E)$ in full line) and for 10 ML porous ice ($g_2(E)$ in dotted line), deduced from the simulation of the whole TPD spectra presented in Fig. 1.

B From compact to porous ice films

The presence of new adsorption sites that are formed as the thickness of the porous overlayer grows can be probed by studying porous ASW samples of intermediate thicknesses (<10 ML). Starting with a previously prepared compact ASW film cooled to 10 K, we have repeated the TPD investigations presented above after successive addition of porous ASW ice layers by background dosing (thicknesses 0.125, 0.25, 0.5, 1, 1.5, 5, 10, 20 ML). As said in the introduction, this process is used for the formation of porous ASW. As an illustration, the TPD series obtained after growing a 1 ML porous ASW film are presented in Fig. 3. The TPD spectra reveal significant desorption above 20 K, clearly correlated to the presence of the new adsorption sites as compared to a pure compact ice film. On the other hand, the overall shapes of the TPD curves do not match those obtained from the 10 ML porous sample. They more accurately appear as a mixture of the two TPD profiles seen for compact and

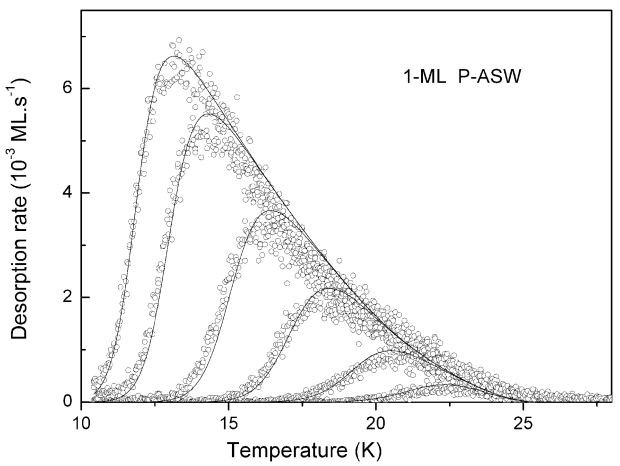

Fig. 3 Temperature-programmed desorption of D_2 from a 1 ML porous ASW film. The film is prepared at 10 K by background deposition on top of a 150 ML compact film deposited at 120 K. Experimental data (circles) and simulated spectra (lines) are compared (see text for details). D_2 exposures are 0.02, 0.08, 0.22, 0.43, 0.72, 0.99 ML.

porous ice (Fig. 1). This suggests using a combination of the two distribution functions found above, in order to describe the effective binding-energy distribution holding at intermediate thicknesses. The analysis of the spectra obtained at various exposures have therefore been simulated by fitting the mixing coefficients α and β of the binding-energy distribution $g(E) = \alpha g_1(E) + \beta g_2(E)$ (where $\alpha + \beta = 1$). The good agreement between simulated and experimental TPD spectra can be seen in Fig. 3. This method has been repeated systematically for several thicknesses of porous ice. The results are summarised in Fig. 4, in which the contribution β for the porous ice distribution is plotted against the number of added porous ice layers on to a compact ice substrate. The magnitude of the porous ice contribution increases very rapidly with water thickness. Within just 1 ML of added porous ice, the spectra can be reproduced with 80% of porous ice energy distribution. Above 5 ML, the contribution of the nonporous surface vanishes entirely. This sharp evolution is markedly observed on the TPD desorption kinetics conducted at low D_2 exposure. As an illustration, Fig. 5 shows a comparison of the TPD spectra obtained at equivalent low D_2 exposures ($\sim$0.02 ML). The TPD curves shift towards higher temperatures with increasing porous ice thickness. A quarter of monolayer of water ice is sufficient to induce a significant shift of the TPD peak. Above 1 ML of additional water, the curves remain very similar, indicating that no more evolution can be seen at this low D_2 dose. In addition, the overlap with the curve initially obtained from the nonporous surface is extremely small. This last property suggests that none of the adsorbed molecules are interacting with the compact base, but that molecules are trapped in the thin added porous part of the film before their desorption. The high sensitivity of the TPD technique to the ice thickness is linked to the very high mobility of deuterium molecules which are able to find the most binding energy sites prior to desorption.[32] Again, this spectacular effect illustrates the immediate contribution of new binding adsorption sites when highly disordered water structures are added onto the compact substrate.

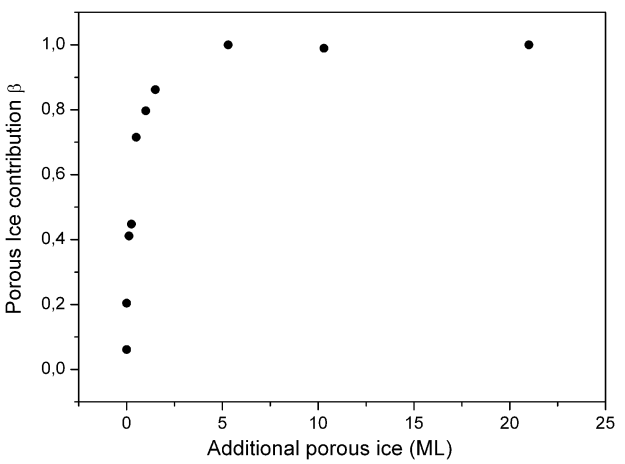

Fig. 4 Relative contribution β of the porous ice binding-energy distribution *versus* porous water ice coverage. The coefficient was obtained by the simulation of TPD spectra (as shown in Fig. 3) using a binding-energy distribution $g(E) = \alpha g_1(E) + \beta g_2(E)$ (where $\alpha + \beta = 1$).

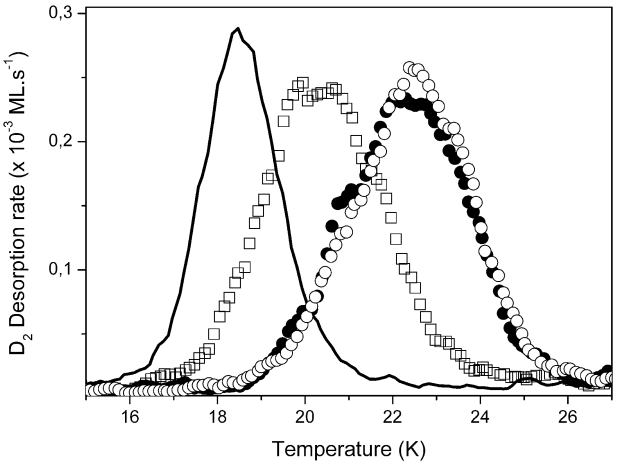

Fig. 5 Comparison of TPD spectra obtained after equivalent D_2 exposure ($\sim$0.02 ML) from compact ice (full line) and from ultra-thin ASW films grown over compact ice: compact + 0.25 ML H_2O (open squares), compact + 0.5 ML H_2O (full circles), compact + 1 ML H_2O (open circles).

Discussion

In this study, we compare the energy distribution of molecular hydrogen adsorbed on compact (nonporous) and porous ice surfaces respectively by using TPD experiments. Besides an increase of the number of adsorption sites when growing porous ice, the energy distribution associated to the porous sample also reveals the existence of a small fraction of more strongly binding sites that are not present at the surface of compact ASW. Specific assignment to well-defined adsorption sites, such as that that can be made for gases adsorbed on crystalline water ice is not possible here. The very high disorder in the morphology of ASW leads to more complex situations. Nevertheless, numerous computational approach simulating amorphous water ices have given much insight into the surface structure of amorphous ices.[11,32–42] Calculations of water clusters were found to reproduce accurately several measured properties of porous systems, such as density and its evolution with temperature.[42] The general shape and energy domain for the D_2 binding-energy distribution calculated with water clusters are in good agreement with those deduced from our TPD experiments conducted on 10 ML porous ASW film.[24,42] At the subnanometre scale, water clusters present numerous cavities and voids, presenting a rough surface characterised by numbers of low-coordinated water molecules on the surface in a strongly distorted hydrogen-bond network. Thus, the wide distribution of binding energy results from several possible geometric configurations of molecular hydrogen relative to the water surface (including distances and orientations), for which the interaction of D_2 (or H_2) with various number of water neighbours is greatly enhanced by the roughness of the surface.

In the present experimental investigation, when the porous film is progressively grown over the compact and nonporous substrate at 10 K, additional water molecules impinging on the surface (with omni-directional angular distribution with respect to the normal of the surface), are expected to almost stick right where they impact the cold surface.[11] Due to their

very limited mobility, new geometric arrangements favouring a stronger interaction with other neighbouring water molecules are not likely. One can expect such a process to produce randomly orientated low-coordinated water molecule at the surface. Numerical simulations of low temperature amorphous deposits based on models of water clusters have given physical insight to the condensation process.[36] These calculations have revealed the preferential sticking of new water molecules to dangling atoms (H atoms not involved in a hydrogen bond or O atoms involved in only one hydrogen bond), giving rise to water molecules that tend to stick out of the surface, and from which surface protuberances can propagate, contributing to the formation of highly corrugated surfaces. Computation have also shown that dangling atoms present on the surface play a role in the interaction with H_2.[37,43,44] Following the picture given by Hixson *et al.*,[43] the deeper binding sites for H_2 adsorbed on amorphous ice lie in the vicinity of the dangling bonds, involving a specific orientation of molecular hydrogen with respect to one dangling atom, together with favourable van der Waals interactions with several neighbouring water molecules. The calculations show that these multiple van der Waals interactions of H_2 with water molecules dominate in fact the surface bonding.[43] Further experimental and computational studies have demonstrated preferential adsorption of *ortho*-H_2 with respect to *para*-H_2, especially in the vicinity of dangling bonds.[44] More recently, we have performed rotationally selective TPD experiments using molecular hydrogen (D_2) adsorbed on a 10 ML porous ASW film.[45] These experiments reveal an excess of the average binding energy of 1.4 meV for *para*-D_2 ($J = 1$) with respect to *ortho*-D_2 ($J = 0$). In the present study, since a mixture of *para*- and *ortho*-D_2 is used, this energy difference contributes to the broadening of the binding-energy distribution found, although this effect is significantly small if compared to the wide range of binding energies available. The binding-energy distribution revealed here, through TPD experiments that are not selective to *ortho* and *para* species, is clearly dominated by the surface morphology.

In the present set of experiments, the D_2 TPD spectra show a very high sensitivity to the presence of a fraction of added water deposited at low temperature (10 K). Especially, a desorption temperature above 21 K is a signature of such an added layer of water. It is particularly striking that the energy distribution of porous ice is clearly dominant above 1 ML (Fig. 4), concurrently with the fact that the appearance of the most energetic adsorption sites seems to be achieved at 1 ML (Fig. 5). This behavior can therefore be used as a basis for the characterization of the morphology of the ice surface with molecular hydrogen, D_2 TPD being an easy and sensitive tool for that purpose. One can note that no evolution of the porous ice contribution can be seen between 5 and 20 ML (Fig. 4). In this range, one unique binding-energy distribution can be used to describe the TPD curves measured for various thicknesses. On the other hand, one can expect that porous ice structure and morphology are not completely achieved at 5 ML. Cavities, voids and pores network of various sizes, involving a large number of water molecules, are probably continuously formed up to 20 ML and above. This behaviour indicates that TPD measurements are merely concerned with local interactions at molecular scale. No direct information about the ice morphology at larger scale can be deduced from these TPD experiments.

Thus, the present experiments confirm the important role, for the porous ice formation, played by low-coordinated water molecule on the surface. The presence of such molecules on the surface initiates local corrugations, providing new energetic binding sites for molecular hydrogen. The results are in line with the picture given by numerical calculations of water clusters, that can be considered as good models for the simulation of initial stages of porous ice formation.[38]

Conclusion

In this study, we have shown how the desorption kinetics of D_2 evolves as the substrate goes from a compact to an ultra-thin layer of porous ASW ice. We found that a very small amount of highly disordered water molecule added over a nonporous substrate is sufficient to create the local environment favouring high energetic binding sites characterizing highly porous ice film. Above $\sim$5 ML, for which most of the compact ice surface is covered by additional water, no additional type of interaction (*i.e.*, more energetic binding sites) is created. One can distinguish two regimes in the evolution of the porous ice contribution with water coverage. A fast regime ($<$1 ML) corresponding to the creation of new energetic adsorption sites and a second regime (1–5 ML) associated to a more gradual redistribution of numerous adsorption sites. Less energetic binding sites might correspond to less coordinated D_2 molecules and interactions with protruding H or O atoms, most sites associated with deeper penetration into the local corrugation of the surface being already filled in higher binding energy wells.[40] The rapid modification of the surface properties of ASW with water thickness that has been revealed in the present study can have important consequences in the context of gas-surface heterogeneous chemistry. These results are very complementary to these recently published by Zubkov *et al.*[29,30] on thicker ASW probed with N_2. Although the TPD signatures were found to peak towards higher temperatures with increasing thicknesses, similarly to what has been found in the present study, the origin of this behaviour is basically different. In the case of very thick ASW, the diffusion and the distribution of molecules within the porous network strongly affect the desorption kinetics. These effects have to be distinguished from the present intrinsic modification of the local structure of the ice film, which directly affect the desorption kinetics of ultra-thin layers.

Acknowledgements

The authors acknowledge support of the national PCMI program funded by the CNRS, as well as the strong financial support from the Conseil Régional d'Ile-de-France (SESAME program E1315) and the Conseil Général du Val d'Oise.

References

1 P. Ehrenfreund, H. J. Fraser, J. Blum, J. H. E. Cartwright, J. M. Garcia-Ruiz, E. Hadamcik, A. C. Levasseur-Regourd,

S. Price, F. Prodi and A. Sarkissian, *Planet. Space Sci.*, 2003, **51**, 473–494.
2 W. Hagen, A. G. G. M. Tielens and J. M. Greenberg, *Chem. Phys.*, 1981, **56**, 367–379.
3 A. Kouchi, T. Yamamoto, T. Kozasa, T. Kuroda and J. M. Greenberg, *Astron. Astrophys.*, 1994, **290**, 1009–1018.
4 M. E. Palumbo, *Astron. Astrophys.*, 2006, **453**, 903–909.
5 R. Papoular, *Mon. Not. R. Astron. Soc.*, 2005, **626**, 489–497.
6 E. Herbst, Q. Chang and H. M. Cuppen, *Journal of Physics: Conference Series*, 2005, **6**, 18–35.
7 L. Amiaud, F. Dulieu, J.-H. Fillion, A. Momeni and J. L. Lemaire, *J. Chem. Phys.*, 2007, **127**, 144709.
8 M. S. Westley, G. A. Baratta and R. A. Baragiola, *J. Chem. Phys.*, 1998, **108**, 3321–3226.
9 K. P. Stevenson, G. A. Kimmel, Z. Dohnálek, R. S. Smith and B. D. Kay, *Science*, 2001, **283**, 1505–1507.
10 G. A. Kimmel, K. P. Stevenson, Z. Dohnálek, R. S. Smith and B. D. Kay, *J. Chem. Phys.*, 2001, **114**, 5284–5294.
11 G. A. Kimmel, Z. Dohnálek, K. P. Stevenson, R. S. Smith and B. D. Kay, *J. Chem. Phys.*, 2001, **114**, 5295–5303.
12 Z. Dohnálek, G. A. Kimmel, P. Ayotte, R. S. Smith and B. D. Kay, *J. Chem. Phys.*, 2003, **118**, 364–372.
13 R. S. Smith, C. Huang, E. K. L. Wong and B. D. Kay, *Phys. Rev. Lett.*, 1997, **79**, 909–912.
14 P. Ayotte, R. S. Smith, K. P. Stevenson, Z. Dohnalek, G. A. Kimmel and B. D. Kay, *J. Geophys. Res., [Atmos.]*, 2001, **106**, 33387–33392.
15 M. P. Collings, J. W. Dever, H. J. Fraser, M. R. S. McCoustra and D. A. Williams, *Astrophys. J.*, 2003, **583**, 1058–1062.
16 E. Mayer and R. Pletzer, *Nature*, 1986, **319**, 298–299.
17 M. P. Collings, M. A. Anderson, R. Chen, J. W. Dever, S. Viti, D. A. Williams and M. R. S. McCoustra, *Mon. Not. R. Astron. Soc.*, 2004, **354**, 1133–1140.
18 K. I. Öberg, F. van Broekhuizen, H. J. Fraser, S. E. Bisschop, E. F. van Dishoeck and S. Schlemmer, *Astrophys. J.*, 2005, **621**, L33–L36.
19 S. E. Bisschop, H. J. Fraser, K. I. Öberg, E. F. van Dishoeck and S. Schlemmer, *Astron. Astrophys.*, 2006, **449**, 1297–1309.
20 K. Acharyya, G. W. Fuchs, H. J. Fraser, E. F. van Dishoeck and H. Linnartz, *Astron. Astrophys.*, 2007, **446**, 1005–1012.
21 L. Amiaud, PhD thesis, Université de Cergy-Pontoise, France, 2006.
22 R. W. Dissly, M. Allen and V. G. Anicich, *Astrophys. J.*, 1994, **435**, 685–692.
23 L. Hornekaer, A. Baurichter, V. V. Petrunin, A. C. Luntz, B. D. Kay and A. Al-Halabi, *J. Chem. Phys.*, 2005, **122**, 124701–124722.
24 L. Amiaud, J.-H. Fillion, S. Baouche, F. Dulieu, A. Momeni and J.-L. Lemaire, *J. Chem. Phys.*, 2006, **124**, 094702.
25 H. Perets, O. Biham, V. Pironello, J. E. Roser, S. Swords, G. Manico and G. Vidali, *Astrophys. J.*, 2005, **627**, 850.
26 P. Jenniskens, D. F. Blake, M. A. Wilson and A. Pohorille, *Astrophys. J.*, 1995, **455**, 389–401.
27 B. Rowland, M. Fisher and J. P. Devlin, *J. Chem. Phys.*, 1991, **95**, 1378–1384.
28 F. Dulieu, L. Amiaud, S. Baouche, A. Momeni, J.-H. Fillion and J.-L. Lemaire, *Chem. Phys. Lett.*, 2005, **404**, 187–191.
29 T. Zubkov, R. S. Smith, T. R. Engstrom and B. D. Kay, *J. Chem. Phys.*, 2007, **127**, 184707.
30 T. Zubkov, R. S. Smith, T. R. Engstrom and B. D. Kay, *J. Chem. Phys.*, 2007, **147**, 184708.
31 D. R. Haynes, N. J. Tro and S. M. George, *J. Phys. Chem.*, 1992, **96**, 8502–8509.
32 E. Matar, E. Congiu, F. Dulieu, A. Momeni and J. L. Lemaire, *Astron. Astrophys.*, 2008, **492**, L17.
33 Q. Zhang and V. Buch, *J. Chem. Phys.*, 1990, **92**, 1512–1513.
34 Q. Zhang and V. Buch, *J. Chem. Phys.*, 1990, **92**, 5004–5016.
35 V. Buch, *J. Chem. Phys.*, 1990, **93**, 2631.
36 V. Buch, *J. Chem. Phys.*, 1992, **96**, 3814–2639.
37 J. P. Devlin and V. Buch, *J. Phys. Chem.*, 1995, **99**, 16534–16548.
38 V. Buch and J. P. Devlin, *Book Series: IAU Symposia; Molecules in Astrophysics: Probes and Processes*, ed. E. F. Van Dishoeck, Springer, 1997, vol. 178, pp. 321–330.
39 U. Essmann and A. Geiger, *J. Chem. Phys.*, 1995, **103**, 4678–4692.
40 A. Al-Halabi, H. J. Fraser, G. J. Kroes and E. F. van Dishoeck, *Astron. Astrophys.*, 2004, **422**, 777–791.
41 A. Al-Halabi, E. F. van Dishoeck and G. J. Kroes, *J. Chem. Phys.*, 2004, **120**, 3358–3367.
42 B. Guillot and Y. Guissani, *J. Chem. Phys.*, 2004, **120**, 4366–4382.
43 H. G. Hixson, M. J. Wojcik, M. S. Devlin, J. P. Devlin and V. Buch, *J. Chem. Phys.*, 1992, **92**, 753–767.
44 V. Buch and J. P. Devlin, *J. Chem. Phys.*, 1993, **98**, 4195–4206.
45 L. Amiaud, A. Momeni, F. Dulieu, J.-H. Fillion, A. Momeni and J. L. Lemaire, *Phys. Rev. Lett.*, 2008, **100**, 053101.

